DOI: 10.38061/idunas.932338

IDUNAS	NATURAL & APPLIED SCIENCES JOURNAL	2021 Vol. 4 No. 2 (16-31)

Infinite Perimeter Selective Segmentation Model

Research Article

Lavdie Rada[1*]

[1]Biomedical Engineering Department, Bahcesehir University, Istanbul, Turkey.

Author E-mails
lavdie.rada@eng.bau.edu.tr

*Correspondance to: Lavdie Rada, Biomedical Engineering Department, Bahcesehir University, Istanbul, Turkey.
DOI: 10.38061/idunas.932338

Received:, 03.06.2021; Accepted: 05.11.2021

Abstract

Accurate boundary determination and segmentation of an object of interest in an image is a difficult image segmentation task. In this paper, we propose a new variational model composed of two penalizations and two fitting terms improving the old selective segmentation models. To better deal with oscillatory boundaries, a $\mathcal{H}^1$ weighted length term and $\mathcal{L}^2$ Lebesgue measure have been employed as penalization terms, whereas the fitting terms consist of a region-based and area fitting term. The model has the same speed as the previous one-level set interactive segmentation models and is much faster compared to previously dual-level set models by having the same segmentation accuracy and reliability. On the other hand, the model shows a good performance while dealing with irregular and oscillatory object boundaries. The comparison with segmentation algorithms of the same nature shows that the proposed model shows the same or improved performance for object segmentation with transparent boundaries or inhomogeneous intensity of the aimed object. Moreover, we show that the proposed model finds the aimed object boundaries successfully for smooth or challenging oscillatory topological structures.
Keywords: Total variation, Edge detection, $\mathcal{L}^2$-Lebesgue measure, Interactive segmentation.

1. INTRODUCTION

Despite developments and improvements in photography and imaging, image post-processing techniques are commonly required. Image segmentation is one such task that separates the object/ objects from their surroundings by extracting aimed boundaries in a meaningful manner. Many applications of image segmentation are observed in a wide range of fields, such as medical imaging, object detection and recognition, traffic control systems, etc.

Segmentation techniques divide into two classes: global and selective/interactive segmentation. The first class aims at the boundary of all objects into a given image scene, whereas the second class aims at the boundary of a specific object. Global segmentation consists of objects' boundaries extraction (foreground) from their surrounding (background). In the last decades, different global segmentation techniques, such as

region-based segmentation, edge-based segmentation, clustering, Mask R-CNN, etc., have been introduced. Variational segmentation models, based on an early idea of representing the image as a piece-wise continuous function [19], easily implemented by Chan-Vese (CV) [7] through the level set function [22], was further used by many segmentation techniques. CV model and further followed improved models prove to be very efficient compared with statistical methods [10, 9, 30], image thresholding [16, 26], wavelet techniques [17, 14,27], etc. Most variational based segmentation approaches in the last decades base their models on edge information to guide the contours towards aimed edges [1, 6, 11, 13] or statistical information for the homogeneous area in the object's region, similar to the CV model [7].

On the other hand, in some particular applications, one single object is required to be segmented. Such examples can be found in medical imaging where a particular organ is required to automatically be segmented or Closed Circuit TV (CCTV) surveillance system where activities monitoring is aimed. The main issue in an interactive/ selective image segmentation problem is how to distinguish one object of interest from similar (nearby) other objects. Recently, variational based models were proposed [3, 13, 18, 25, 24]. Those models combine edge detection function with distance metrics to form some geometric priors information (markers). Such work was introduced by Rada et al. [25] where a dual-level set is used for boundaries detection (a local level set evolves over a global level set to detect the boundaries on the aimed target object). The model show improvement compared to other models of the same type by being more reliable for cases where the intensity difference between objects is small. Although this model [25] is reliable, the model does not perform well for oscillatory boundaries. To improve the model for such boundaries a new dual-level set model was introduced by the same authors [24]. The new model [24] improves the old model by using the $\mathcal{L}^2$ Lebesgue measure of the γ-neighborhood of the contour [4] replacing the $\mathcal{H}^1$ Hausdorff measure [25] as penalization term. Both these models are slow because of the complexity of the incorporation of the two level set functions. To improve the dual-level set work [25], Rada et al. [24] introduced a new variational area fitting based model. This model is fast and reliable but has slight difficulties with specific cases where the aimed objects have oscillatory boundaries. The purpose of the following presented work consist of the design of a new single level-set model which yet ensuring the same or better performance for oscillatory boundaries compared to Rada et al. [24] model.

Furthermore, we should emphasize that for image data where prior information is provided different machine learning and pattern recognition algorithms can be employed [5, 2, 8]. However, their large training sets and parameters optimization through the architecture layers makes them limited for previously unseen object classes. In this paper, we consider the cases where prior data is not available and the method can be easily adapted for general cases.

The following sections are organized in the following way. Section 2 contains a review of some selective segmentation models. In Section 3, we present the proposed $\mathcal{L}^2$ Lebesgue measure based model. Then, in Section 4, the discretization of the derived partial differential question through an additive operator splitting (AOS) algorithm is described, ist efficiency and speed. In Section 5, we provide experimental results and comparisons to some existing methods for different images. We conclude our work in Section 6.

2. A SHORT REVIEW ON SOME INTERACTIVE/SELECTIVE SEGMENTATION MODELS

The introduction of a level set idea by Chan-Vese (CV) [7] led to a simple and easy numerical representation of the Mumford-Shah [20] variational image segmentation model. Using Chan-Vese (CV) [7] idea many segmentation models were introduced in the last decades. Given an image $u_0(\boldsymbol{x})$, $x \in \Omega$ defined on a rectangular domain Ω, the CV model restricts the image into a piecewise function to be

represented with a two-phase level set function. The piecewise function consists of two values c_1 and c_2 that represent the mean intensity value of the foreground and the background, respectively. The CV model is not based on the gradient of the image for the stopping process so that it can detect contours both with and without gradients. The energy minimization functional in terms of level set is given as follows:

$$\min_{c_1,c_2,\Gamma} F(\Gamma, c_1, c_2) = \min_{c_1,c_2,\Gamma} \{\mu_{cv}\text{length}(\Gamma) + \lambda_{1cv} \int_{\text{inside }(\Gamma)} |u_0(\mathbf{x}) - c_1|^2 d\mathbf{x}$$

$$+ \lambda_{2cv} \int_{\text{outside }(\Gamma)} |u_0(\mathbf{x}) - c_2|^2 d\mathbf{x}\} \quad (1)$$

where c_1 and c_2 are the average values of $u_0(\boldsymbol{x})$ inside and outside of the variable contour Γ, also μ, λ_1 and λ_2 are non-negative fixed parameters. Writing the level set function $\phi: \Omega \to \mathbb{R}$

$$\begin{cases} \Gamma = \partial\Omega_1 = \{(\boldsymbol{x}) \in \Omega |\ \phi(\boldsymbol{x}) = 0\}, \\ \text{inside}(\Gamma) = \Omega_1 = \{\boldsymbol{x} \in \Omega |\ \phi(\boldsymbol{x}) > 0\}, \\ \text{outside}(\Gamma) = \Omega_2 = \{\boldsymbol{x} \in \Omega |\ \phi(\boldsymbol{x}) < 0\}, \end{cases}$$

the energy function (1) is written in the form:

$$F(\phi, c_1, c_2) = \mu_{cv} \int_\Omega |\nabla H(\phi)| d\boldsymbol{x} + \lambda_{1cv} \int_\Omega |u_0(\boldsymbol{x}) - c_1|^2 H\big(\phi(\boldsymbol{x})\big) d\boldsymbol{x}$$
$$+\lambda_{2cv} \int_\Omega |u_0(\boldsymbol{x}) - c_2|^2 (1 - H(\phi(\boldsymbol{x}))) d\boldsymbol{x}, \quad (2)$$

where H defines the Heaviside function

$$H(x) = \begin{cases} 1 & \text{if } x \geq 0 \\ 0 & \text{if } x < 0. \end{cases}$$

In the following we review selective segmentation models related to the new proposed work.

Dual Level Set Selective Segmentation Model for Oscillatory Boundaries With Infinite Perimeter Norm

As an attempt to improve the dual level set model [25] for segmentation of objects with irregular boundaries, the work of Rada et al. [24] replaces the $\mathcal{H}^1$ length term in the old Rada et al. work [25] with the γ-neighborhood area of the contour Γ (following the Barchiesi et al. [4] approach for global segmentation). The γ-neighborhood area of the contour of the edge set Γ is given as follows [4]

$$\gamma - \Gamma := \cup_{x \in \Gamma} B_\gamma(x). \quad (3)$$

This $\mathcal{L}^2$ measure plays an important role in capturing inperfect oscillating boundaries boundaries of the foregrownd objects in the given image $u_0(x)$ while achieving the denoising effect [4]. Considering $f_0 := \chi_{0,1]}$, and a smooth version of it f, such as $f(t) = e^{-t^k}$ or $f(t) = \frac{1}{1+t^k}$ for $k \geq 1$, the $\mathcal{L}^2(\gamma - \Gamma)$ term can be rewritten as:

$$\mathcal{L}^2(\gamma - \Gamma) := \int_\Omega f_0\left(\frac{dist\,(x,\Gamma)}{\gamma}\right) dx \approx \int_\Omega f\left(\frac{dist\,(x,\Gamma)}{\gamma}\right) dx. \quad (4)$$

In the presented work of Rada et al. [24], the $\mathcal{L}^2(\gamma - \Gamma)$ is approximated as

$$\mathcal{L}^2(\gamma - \Gamma) \approx \int_\Omega e^{-\frac{\phi(h)^k}{\gamma^k}},$$

for large value of the parameter k. Following similar problem to the level set selective segmentation models [3, 11, 13, 25], a set of geometrical points $\mathcal{A} = \{w_i^* = (x_i^*, y_i^*) \in \Omega, 1 \leq i \leq n_1\} \subset \Omega$, consisting of n_1 distinct points near the object, has been defined. Using the Lipschitz level set function the energy function of this model is given as following:

$$\min_{\phi_L(\mathbf{x}),\phi_G(\mathbf{x}),c_1,c_2} F_{IDLSS}(\phi_L,\phi_G,c_1,c_2) =$$
$$\mu_1 \int_\Omega D(\mathbf{x})g(\nabla u_0)e^{-(\frac{\phi_L}{\gamma})^k} H(\phi_G) + \frac{\mu_L}{2}\int_\Omega (|\nabla\phi_L| - 1)^2 d\mathbf{x} \; +$$
$$\mu_2 \int_\Omega g(\nabla u_0)e^{-(\frac{\phi_G}{\gamma})^k} + \frac{\mu_G}{2}\int_\Omega (|\nabla\phi_G(\mathbf{x})| - 1)^2 d\mathbf{x} \; + \qquad (5)$$
$$\lambda_{1G}\int_\Omega |u_0(\mathbf{x}) - c_1|^2 H(\phi_G(\mathbf{x})d\mathbf{x} \; + \lambda_{2G}\int_\Omega |u_0(\mathbf{x}) - c_2|^2(1 - H(\phi_G(\mathbf{x}))d\mathbf{x} \; +$$
$$\lambda_1 \int_\Omega |u_0(\mathbf{x}) - c_1|^2 H(\phi_L(\mathbf{x})d\mathbf{x} \; + \lambda_2 \int_\Omega |u_0(\mathbf{x}) - c_1|^2(1 - H)(\phi_L(\mathbf{x}))H(\phi_G(\mathbf{x})d\mathbf{x} \; +$$
$$\lambda_3 \int_\Omega |u_0(\mathbf{x}) - c_2|^2(1 - H)(\phi_L(\mathbf{x}))(1 - H(\phi_G(\mathbf{x}))d\mathbf{x}.$$

where ϕ_L, ϕ_G, are the local level set and global level set, respectively, $D(\mathbf{x})$ and $g(\mathbf{x})$, are the distance and edge detection functions, respectively. Both $D(\mathbf{x})$ and $g(\mathbf{x})$ function has a property of approaching zero while aproaching near the Γ boundary and has big value when away from it. The global level set detect all the boundaries of the objects in the given image whereas the local level set evolves over the global level set in order to detect the aimed object near the given geometric set of points. The constants $\mu_1, \mu_2, \lambda_{1G}, \lambda_{2G}, \mu_L, \mu_G, \lambda_1, \lambda_2, \lambda_3$, are defined parameters related to the model. The functions $H(\phi_L)$, and $H(\phi_G)$ represent the local and global level set functions corresponding to the local and global level set.

To tackle the discontinuity issue in 0 of the Heaviside function, regularized Heaviside functions can be used such as $H_\epsilon = \frac{1}{2}(1 + \frac{2}{\pi}\arctan(\frac{z}{\epsilon}))$. In this way the above model can be written:

$$\min_{\phi_L(\mathbf{x}),\phi_G(\mathbf{x}),c_1,c_2} F_{IDLSS}(\phi_L,\phi_G,c_1,c_2) =$$
$$\mu_1 \int_\Omega D(\mathbf{x})g(\nabla u_0)e^{-(\frac{\phi_L}{\gamma})^k} H_\epsilon(\phi_G) + \frac{\mu_L}{2}\int_\Omega (|\nabla\phi_L| - 1)^2 d\mathbf{x} \; +$$
$$\mu_2 \int_\Omega g(\nabla u_0)e^{-(\frac{\phi_G}{\gamma})^k} + \frac{\mu_G}{2}\int_\Omega (|\nabla\phi_G(\mathbf{x})| - 1)^2 d\mathbf{x} \; + \qquad (6)$$
$$\lambda_{1G}\int_\Omega |u_0(\mathbf{x}) - c_1|^2 H_\epsilon(\phi_G(\mathbf{x})d\mathbf{x} \; + \lambda_{2G}\int_\Omega |u_0(\mathbf{x}) - c_2|^2(1 - H_\epsilon(\phi_G(\mathbf{x}))d\mathbf{x} \; +$$
$$\lambda_1 \int_\Omega |u_0(\mathbf{x}) - c_1|^2 H_\epsilon(\phi_L(\mathbf{x})d\mathbf{x} \; + \lambda_2 \int_\Omega |u_0(\mathbf{x}) - c_1|^2(1 - H_\epsilon(\phi_L(\mathbf{x}))H(\phi_G(\mathbf{x})d\mathbf{x} \; +$$
$$\lambda_3 \int_\Omega |u_0(\mathbf{x}) - c_2|^2(1 - H_\epsilon(\phi_L(\mathbf{x}))(1 - H_\epsilon(\phi_G(\mathbf{x}))d\mathbf{x}.$$

By keeping ϕ_L and ϕ_G fixed and deriving with respect to c_1 and c_2, one get equations for computing c_1 and c_2:

$$c_1 = \frac{\lambda_{1G}\int_\Omega u_0 H_\epsilon(\phi_G)d\mathbf{x} + \lambda_1\int_\Omega u_0 H_\epsilon(\phi_L)d\mathbf{x} + \lambda_2\int_\Omega u_0(1 - H_\epsilon(\phi_L))H_\epsilon(\phi_G)d\mathbf{x}}{\lambda_{1G}\int_\Omega H_\epsilon(\phi_G)d\mathbf{x} + \lambda_1\int_\Omega H_\epsilon(\phi_L)d\mathbf{x} + \lambda_2\int_\Omega (1 - H_\epsilon(\phi_L))H_\epsilon(\phi_G)d\mathbf{x}}, \qquad (7)$$

$$c_2 = \frac{\lambda_{2G}\int_\Omega u_0(1 - H_\epsilon(\phi_G))d\mathbf{x} + \lambda_3\int_\Omega u_0(1 - H_\epsilon(\phi_L))(1 - H_\epsilon(\phi_G))d\mathbf{x}}{\lambda_{2G}\int_\Omega (1 - H_\epsilon(\phi_G))d\mathbf{x} + \lambda_3\int_\Omega (1 - H_\epsilon(\phi_L))(1 - H_\epsilon(\phi_G))d\mathbf{x}}, \qquad (8)$$

and by keeping c_1 and c_2 fixed we get the equations for ϕ_G and ϕ_L

$$\begin{cases} \mu_2 g(\nabla u_0)\frac{k}{\gamma^k}\phi_G^{k-1}e^{-(\frac{\phi_G}{\gamma})^k} + \mu_G\nabla\cdot((1-\frac{1}{|\nabla\phi_G|})\nabla\phi_G) + \\ \delta_\epsilon(\phi_G)(-\mu_1 d(\mathbf{x})g(\nabla u_0)e^{-(\frac{\phi_L}{\gamma})^k} - \lambda_{1G}(u_0(\mathbf{x})-c_1)^2 + \lambda_{2G}(u_0(\mathbf{x})-c_2)^2 - \\ \lambda_2(u_0(\mathbf{x})-c_1)^2(1-H(\phi_L)) + \lambda_3(u_0(\mathbf{x})-c_2)^2(1-H(\phi_L))) \;+\; \alpha g(\mathbf{x})|\nabla\phi_G| = 0, \text{in } \Omega \\ \frac{\partial\phi_G}{\partial\vec{n}} = 0 \text{ on } \partial\Omega. \end{cases} \tag{9}$$

and

$$\begin{cases} \mu_1 D(\mathbf{x})g(\nabla u_0)\frac{k}{\gamma^k}\phi_L^{k-1}e^{-(\frac{\phi_L}{\gamma})^k}H_\epsilon(\phi_G) + \mu_L\nabla\cdot((1-\frac{1}{|\nabla\phi_L|})\nabla\phi_L) + \\ \delta_\epsilon(\phi_L)(-\lambda_1(u_0(\mathbf{x})-c_1)^2 + \lambda_2(u_0(\mathbf{x})-c_1)^2 H_\epsilon(\phi_G) + \\ \lambda_3\left(u_0(\mathbf{x})-c_2)^2(1-H_\epsilon(\phi_G)\right)\right) \;+\; \alpha d(\mathbf{x})g(\nabla u_0)|\nabla\phi_L| = 0, \text{in}\Omega \\ \frac{\partial\phi_L}{\partial\vec{n}} = 0 \text{ on } \partial\Omega, \end{cases} \tag{10}$$

The terms $\alpha g(x,y)|\nabla\phi_G|$ and $\alpha d(x,y)g(\nabla u_0)|\nabla\phi_L|$ are the balloon term force.

Area Based Selective Segmentation Model

Rada et al. [23] introduced a simple and fast variational model for the interactive/ selective segmentation task. This model improved the old dual-level set model [25]. This method is based on a Euclidean distance from the manually given points combined with an area-based fitting term and an adaptive parameter edge detection function, which tends to 0 as soon as the contour reaches the boundaries. Given an image $u_0(x)$, defined on the domain Ω, the detection of an aimed feature/object nearby some given points $\mathcal{A} = \{w_i^* = (x_i^*, y_i^*) \in \Omega, 1 \le i \le n_1\} \subset \Omega$, is given in the following form:

$$\begin{aligned} \min_{\Gamma,c_2} F(\Gamma, c_2) \;&= \min_{\Gamma,c_2}\{\mu\int_\Gamma W(|\nabla u_0(\mathbf{x})|)d\mathbf{x} \;+ \\ &\lambda_1\int_{inside\,(\Gamma)}|u_0(\mathbf{x})-c_1|^2 d\mathbf{x} \;+\lambda_2\int_{outsite\,(\Gamma)}|u_0(\mathbf{x})-c_2|^2 d\mathbf{x} \;+ \\ &\nu\{(\int_{inside\,(\Gamma)} d\mathbf{x} - A_1)^2 + (\int_{outsite\,(\Gamma)} d\mathbf{x} - A_2)^2\}, \end{aligned} \tag{11}$$

where $\lambda_1, \lambda_2, \mu$ and ν are empirical weights, $W = D \cdot g$ is the edge detector distance function, c_1 is the mean intensity of constructed polygon with the given points, c_2 is a region term representing the mean intensity outside the target object. The area fitting term, represented in the last row of the last equation, tend to minimize the difference between the area obtained by the evolving level set of the aimed object and the approximated area obtained by the polygon of the given geometric markers. This term serves as a ration constraint between the aimed object and the rest of the image rather than precise area-preserving. The function g is an edge detection function given by:

$$g(|\nabla u_0(\mathbf{x})|) = \frac{1}{1+k|\nabla u_0(\mathbf{x})|^2}, \tag{12}$$

with k a positive constant which can be manualy adapted. Replacing the Heaviside function H with a continuous regularized function H_ϵ, similar to [1, 7] one get:

$$\min_{\phi(x),c_2} F_\epsilon(\phi(\boldsymbol{x}),c_2) = \mu\int_\Omega W(|\nabla u_0(\boldsymbol{x})|)\delta_\epsilon(\phi(\boldsymbol{x}))|\nabla(\phi(\boldsymbol{x}))|d\boldsymbol{x} + \lambda_1\int_\Omega |u_0(\boldsymbol{x})-c_1|^2 H_\epsilon(\phi(\boldsymbol{x}))d\boldsymbol{x} + \lambda_2\int_\Omega |u_0(\boldsymbol{x})-c_2|^2(1-H_\epsilon(\phi(\boldsymbol{x})))d\boldsymbol{x} + \nu\{(\int_\Omega H_\epsilon(\phi(\boldsymbol{x}))d\boldsymbol{x}-A_1)^2 + (\int_\Omega (1-H_\epsilon(\phi(\boldsymbol{x}))d\boldsymbol{x})-A_2)^2\}d\boldsymbol{x}, \quad (13)$$

where $\delta_\epsilon(\phi(\boldsymbol{x}))$ is a Delta function corresponding to the Heaviside function introduced above. Considering that the geometrical points are given inside the aimed object c_1 is computed as the mean intensity of the constructed polygon with those points. Keeping $\phi(x)$ fixed and minimizing with respect to the unknown intensity outside the object, one gets the following equations for computing c_2:

$$c_2(\phi(\boldsymbol{x})) = \frac{\int_\Omega u_0(\boldsymbol{x})(1-H_\epsilon(\phi(\boldsymbol{x})))d\boldsymbol{x}}{\int_\Omega (1-H_\epsilon(\phi(\boldsymbol{x})))d\boldsymbol{x}} \quad (14)$$

if $\int_\Omega (1-H_\epsilon(\phi(\boldsymbol{x})))d\boldsymbol{x} > 0$ (i.e if the curve is nonempty in Ω).

Considering c_1 and c_2 fixed and minimizing (18) with respect to $\phi(\boldsymbol{x})$ and get the following Euler-Lagrange equation:

$$\delta_\epsilon(\phi)\{\mu\nabla\cdot(W\frac{\nabla\phi}{|\nabla\phi|}) - [\lambda_1(u_0(\boldsymbol{x})-c_1)^2 - \lambda_2(u_0(\boldsymbol{x})-c_2)^2] - \nu[(\int_\Omega H d\mathbf{x}-A_1) - (\int_\Omega (1-H)d\mathbf{x}-A_2)]\} = 0, \text{in}\Omega \quad (15)$$
$$\text{with}\frac{\partial\phi}{\partial\vec{n}} = 0, \text{on}\partial\Omega,$$

To speed up the convergence in equation (20) a balloon term, such as $\alpha W|\nabla\phi|$, can be optionaly added. The final equations of ϕ can be written in the form:

$$\delta_\epsilon(\phi)\{\mu\nabla\cdot(W\frac{\nabla\phi}{|\nabla\phi|}) - [\lambda_1(u_0(\boldsymbol{x})-c_1)^2 - \lambda_2(u_0(\boldsymbol{x})-c_2)^2] - \nu[(\int_\Omega H d\mathbf{x}-A_1) - (\int_\Omega (1-H)d\mathbf{x}-A_2)]\} - \alpha W|\nabla\phi| = 0. \quad (16)$$

3. PROPOSED METHOD

In this section, we detail the proposed single level selective segmentation model, useful for oscillatory boundaries which has a better speed performance compared to the previously proposed dual level set model [24]. For a given image $u_0(\mathbf{x})$, defined on the domain Ω, we aim to detect a feature/object of an image nearby the geometrical marked points $\mathcal{A}$, placed nearby the aimed object boundaries. To achieve a correct detection of the aimed irregular boundary object we incorporate: i) a distance-edge detection function incorporated in the smoothing term providing a value $\simeq 0$ while approaching the aimed object; ii) an area-based fitting term providing conditioning the detected area to be is in the same range with the aimed object; iii) an $\mathcal{L}^2$-Lebesgue length term evaluating the area of the γ −neighborhood of the edge set Γ capable to deal with noise, preserve the cornering effect and keeping oscillatory boundaries; iv) $\mathcal{H}^1$ weighted length of the contour. The proposed model is given in the following form:

$$\min_{\Gamma,c_2} F(\Gamma,c_2) = \min_{\Gamma,c_2}\{\mu\int_\Gamma W(|\nabla u_0(\mathbf{x})|)d\mathbf{x} + \mu_1\int_\Omega f(\frac{dist(\mathbf{x},\Gamma)}{\gamma})d\mathbf{x} + \lambda_1\int_{inside(\Gamma)} |u_0(\mathbf{x})-c_1|^2 d\mathbf{x} + \lambda_2\int_{outsite(\Gamma)} |u_0(\mathbf{x})-c_2|^2 d\mathbf{x} + \quad (17)$$

$$\nu\{(\int_{inside\ (\Gamma)} d\mathbf{x} - A_1)^2 + (\int_{outsite\ (\Gamma)} d\mathbf{x} - A_2)^2\},$$

where $\mu, \mu_1, \lambda_1, \lambda_2$ and ν are empirical weights, $W = D \cdot g$ is the edge detector distance function, c_1 is the mean intensity of the constructed polygon with the given markers, c_2 is a region term defined in equation (14) representing the mean intensity outside the target object. As the level set function becomes irregular during computation, optionaly, one can add a fitting terms in order to avoid reinitialization of the level set function $\phi(\mathbf{x})$, e.g. the term $\int_\Omega (|\nabla\phi(\boldsymbol{x})| - 1)^2$ provides the authomatic scale of the level set.

Compering to [23] model one can notice the that the above energy improves [23] model by adding a term similar to the work of [4], capable to deal with oscillatory boundaries. Rewriting the above equation in terms of the level-set, replacing the Heaviside function with the regularized Heaviside function H_ϵ similar to [1, 7], and adding the reinatioalization term for the ϕ level set one get:

$$\begin{aligned}\min_{\phi(x),c_2} F(\phi(\boldsymbol{x}), c_2) \quad &= \mu \int_\Omega g(|\nabla u_0(\boldsymbol{x})|)|\nabla H_\epsilon(\phi(\boldsymbol{x}))|d\boldsymbol{x} + \\ &\mu_1 \int_\Omega G(|\nabla u_0(\mathbf{x})|)g(\nabla u_0)e^{-\frac{\phi^k}{\gamma}} d\mathbf{x} + \mu_2 \int_\Omega (|\nabla\phi(\boldsymbol{x})| - 1)^2 + \\ &\lambda_1 \int_\Omega |u_0(\boldsymbol{x}) - c_1|^2 H_\epsilon(\phi(\boldsymbol{x}))d\boldsymbol{x} \ + \lambda_2 \int_\Omega |u_0(\boldsymbol{x}) - c_2|^2(1 - H_\epsilon(\phi(\boldsymbol{x})))d\boldsymbol{x} + \\ &\nu\{(\int_\Omega H_\epsilon(\phi(\boldsymbol{x}))d\boldsymbol{x} - A_1)^2 + (\int_\Omega (1 - H_\epsilon(\phi(\boldsymbol{x}))d\boldsymbol{x}) - A_2)^2\}d\boldsymbol{x}. \end{aligned} \tag{18}$$

if $\int_\Omega (1 - H_\epsilon(\phi(x)))dx > 0$. Keeping ϕ fixed we update

$$c_2(\phi(\boldsymbol{x})) = \frac{\int_\Omega u_0(\boldsymbol{x})(1 - H_\epsilon(\phi(\boldsymbol{x})))d\boldsymbol{x}}{\int_\Omega (1 - H_\epsilon(\phi(\boldsymbol{x})))d\boldsymbol{x}}. \tag{19}$$

Keeping c_1 and c_2 fixed and minimizing (18) with respect to $\phi(\boldsymbol{x})$ one gets the following equation:

$$\begin{aligned}\delta_\epsilon(\phi)\{\mu\nabla \cdot (W\frac{\nabla\phi}{|\nabla\phi|}) + \quad &\mu_1 \frac{k}{\gamma^k}\phi^{k-1}e^{-(\frac{\phi}{\gamma})^k} H_\epsilon + \mu_2\nabla \cdot ((1 - \frac{1}{|\nabla\phi|})\nabla\phi) - \\ &[\lambda_1(u_0(\boldsymbol{x}) - c_1)^2 - \lambda_2(u_0(\boldsymbol{x}) - c_2)^2] - \\ &\nu[(\int_\Omega H d\mathbf{x} - A_1) - (\int_\Omega (1 - H)d\mathbf{x} - A_2)]\} = 0, \text{in}\Omega \\ &\text{with}\ \frac{\partial\phi}{\partial\vec{n}} = 0, \text{on}\partial\Omega,\end{aligned} \tag{20}$$

4. METHOD DISCRETIZATION AND SOLUTION THROUGH AN ADDITIVE OPERATOR

To solve equation (20), we employ an additive operator splitting (AOS) method known for its properties of fast and low computational cost. AOS splits the two-dimensional problem into the solution of sequential of two one-dimensional ones. The AOS method is proposed by Tai et al. [15] and Weickert [29] has been widely applied in similar diffusion equations, see [3, 13, 28]. In the following, we detail the implementation of the AOS algorithm for the proposed method. The first step of the AOS method is the discretization of the given minimization problem in equation (20). In our work central finite differences has been used. Then form a semi-implicit linear system which leads to an iterative approximation scheme with a tridiagonal diagonally dominant matrix. Recalling equation (20) of the proposed method one can write the gradient descent method as follows:

$$\begin{cases}\phi(\mathbf{x},0)=\phi^0(\mathbf{x})\\ \frac{\partial\phi}{\partial t}=\mu\delta_\epsilon(\phi)\nabla\cdot(W\frac{\nabla\phi}{|\nabla\phi|})+\mu_1\frac{k}{\gamma^k}\phi_G^{k-1}e^{-(\frac{\phi_G}{\gamma})^k}+\mu_2\nabla\cdot((1-\frac{1}{|\nabla\phi|})\nabla\phi)+\\ \delta_\epsilon(\phi)\{-[\lambda_1(u_0(\mathbf{x})-c_1)^2-\lambda_2(u_0(\mathbf{x})-c_2)^2]-\\ \nu[(\int_\Omega Hd\mathbf{x}-A_1)-(\int_\Omega(1-H)d\mathbf{x}-A_2)]\}=0,\end{cases} \tag{21}$$

As singularity may be shown, due to the $|\nabla\phi|$ term in the denominator, we replace the term with $|\nabla\phi|_\beta=\sqrt{\phi_x^2+\phi_y^2+\beta}$, for a small β. Denoting $E=\frac{W}{|\nabla\phi|_\beta}, F=1-\frac{1}{|\nabla\phi|}$ and

$$\begin{aligned}f=\ &\mu_1\frac{k}{\gamma^k}\phi^{k-1}e^{-(\frac{\phi}{\gamma})^k}+\delta_\epsilon(\phi)\{-[\lambda_1(u_0(\mathbf{x})-c_1)^2-\lambda_2(u_0(\mathbf{x})-c_2)^2]\ -\\ &\nu[(\int_\Omega Hd\mathbf{x}-A_1)-(\int_\Omega(1-H)d\mathbf{x}-A_2)]\}\end{aligned} \tag{22}$$

equations (21) can be written in the compact form:

$$\begin{cases}\frac{\partial\phi}{\partial t}=\mu\delta_\epsilon(\phi)\nabla\cdot(E\nabla\phi)+\mu_2\nabla\cdot(F\nabla\phi)+f=\\ \mu\delta_\epsilon(\phi)(\partial_x(E\partial_x\phi)+\partial_y(E\partial_y\phi))+\mu_2\delta_\epsilon(\phi)(\partial_x(F\partial_x\phi)+\partial_y(F\partial_y\phi))+f.\end{cases} \tag{23}$$

Discretizing respect to time the equation (23) can be rewritten in the matrix-vector form:

$$\frac{\phi^{n+1}-\phi^n}{\Delta t}=\sum_{l=1}^2 A_l(\phi^n)\phi^{n+1}+f$$

where Δt is the time step size, n denotes the n^{th} iteration and A_l is the diffusion quantity in the l direction ($l=1$ and $l=2$ respectively for x and y direction for the two dimensional case). The above equation can be written in the semi-implicit form:

$$\phi^{n+1}=(\ I-\Delta t\sum_{l=1}^m A_l(\phi^n))^{-1}\hat{\phi}^n \text{ for } l=1,2 \text{ and } \widehat{\phi}^n=\phi^n+\Delta t f.$$

Using the AOS scheme and its additively split the above equation can be written:

$$\phi^{n+1}=\frac{1}{2}\sum_{l=1}^2(\ I-2\Delta t A_l(\phi^n))^{-1}\hat{\phi}^n \tag{24}$$

Here the matrices A_l, for $l=1,2$, are obtained by using the finite differences scheme as bellow:

$$(A_1(\phi^n)\phi^{n+1})_{i,j}=\mu\delta_\epsilon(\phi^n)(\partial_x(E\partial_x\phi^{n+1})_{i,j}+\mu_2(\partial_x(F\partial_x\phi^{n+1})_{i,j}=$$

$$\mu\delta_\epsilon(\phi^n)\frac{E^n_{i+\frac{1}{2},j}(\partial_x\phi^{n+1})_{i+\frac{1}{2},j}-E^n_{i-\frac{1}{2},j}(\partial_x\phi^{n+1})_{i-\frac{1}{2},j}}{h_x}+$$

$$\mu_2\frac{F^n_{i+1/2,j}(\partial_x\phi^{n+1})_{i+1/2,j}-F^n_{i-1/2,j}(\partial_x\phi^{n+1})_{i-1/2,j}}{h_x}+$$

$$\mu\delta_\epsilon(\phi^n)\frac{\frac{E^n_{i+1,j}+E^n_{i,j}}{2}(\frac{\phi^{n+1}_{i+1,j}-\phi^{n+1}_{i,j}}{h_x})-\frac{E^n_{i,j}+E^n_{i-1,j}}{2}(\frac{\phi^{n+1}_{i,j}-\phi^{n+1}_{i-1,j}}{h_x})}{h_x}+$$

$$\mu_2 \frac{\frac{F^n_{i+1,j}+F^n_{i,j}}{2}\left(\frac{\phi^{n+1}_{i+1,j}-\phi^{n+1}_{i,j}}{h_x}\right)-\frac{F^n_{i,j}+F^n_{i-1,j}}{2}\left(\frac{\phi^{n+1}_{i,j}-\phi^{n+1}_{i-1,j}}{h_x}\right)}{h_x} =$$

$$\mu\delta_\epsilon(\phi^n)\frac{E^n_{i+1,j}+E^n_{i,j}}{2h_x^2}(\phi^{n+1}_{i+1,j}-\phi^{n+1}_{i,j})-\mu\delta_\epsilon(\phi^n)\frac{E^n_{i,j}+E^n_{i-1,j}}{2h_x^2}(\phi^{n+1}_{i,j}-\phi^{n+1}_{i-1,j})+$$

$$\mu_2\frac{F^n_{i+1,j}+F^n_{i,j}}{2h_x^2}\left(\phi^{n+1}_{i+1,j}-\phi^{n+1}_{i,j}\right)-\mu_2\frac{F^n_{i,j}+F^n_{i-1,j}}{2h_x^2}\left(\phi^{n+1}_{i,j}-\phi^{n+1}_{i-1,j}\right),$$

with A_1 is a tridiagonal matrice. Similarly we compute $(A_2(\phi^n)\phi^{n+1})_{i,j}$. The algorithm (1) describes the scheme of the proposed method.

Algorithm 1. Infinite Perimeter Area Fitting Selective Method Algorithm:
$\phi^k \leftarrow IPAFSM(\phi^{(0)}, \mathcal{A}, \mu, \nu, \beta, \alpha, \epsilon, maxit, tol)$.

Compute the distance function D (optional), the edge function g, the area of the polygon, f from equation (22), $\phi^{(1)} = \phi^{(0)}$;

for $iter = 1 : maxit$ **do**

Calculate $\phi^{(n)}$ from (24):

$\phi_l^{(n+1)} \leftarrow \frac{1}{2}\sum_{l=1}^{2}\ (\ I - 2\Delta t A_l(\phi^n))^{-1}\hat{\phi}^n$

If $\| \phi^{(n+1)} - \phi^{(n)} \| < tol$ or $iter > maxit$, set $\phi^{(k)} \leftarrow \phi^{(n-1)}$ Break;

else $\phi^{(n)} \leftarrow \phi^{(n-1)}$

update f from equation (22)

end for

---

5. EXPERIMENTAL RESULTS

In this section, we first argue the robustness of the proposed model for images with regular and oscillatory boundaries type of contours. The initial curve as the model suggests it is placed as near possible inside the given object by using the given markers to construct the zero level set (a polygon passing through the markers). Comparison with a similar one level set selective segmentation model, such as the Rada et al. [23] or Nguyen et al. [21] model has been shown. We perform experiments of our new method by using objects where oscillation boundaries are found. We compare the obtained results of the detected object of such boundaries with the dual-level set selective segmentation model with the infinite perimeter fitting term introduced by Rada et al. [24]. This comparison shows the speed advantage of the proposed method while keeping the same accuracy performance. Furthermore, we show the practical use of this model and its applications in fields such as medicine, where qualitative segmentations are of a great importance. Different size images, such as n = 128 (i.e. 128 × 128), n = 180 (i.e. 180 × 180), and n = 256 (i.e. 256 × 256) , n = 512 (i.e. 512 × 512) , has been used. The parameters k, γ, λ_1, λ_2, μ, μ_1, μ_2 and β used in the following tested experiments are fixed to the values k = 8, γ = 10, $\lambda_1 = \lambda_2$ = 100, μ = 1, μ_1 = 1, μ_2 = 0.0001, ϵ = 1, and $\beta = 10^{-6}$. Based on the quality that the AOS algorithm is unconditionally related to the time step size we use Δt = 1 in all our experiments and a relative residual of 10^{-2}.

Test Set 1 — Segmentation Accuracy and Its Comparison to Other Models

The first test set demonstrates the ability to properly segment objects with different shapes and intensity and then compare with Rada et al. [23] and Nguyen et al. [21]. Fig. 1 shows the segmentation result for two synthetic and two real-life images. The aimed object in the first image in Fig. 1 is a square placed nearby to an *L* shape geometrical object with the same intensity. The second image of this figure contains a geometrical object which has to be separated from the other geometrical objects. Furthermore, the object itself is not homogeneous inside the given geometrical markers (white background is found between the object itself). The third and the fourth images are knee and cell images with a high level of noise. From Fig. 1 we can easily notice that the proposed method correctly captured the aimed objects. We have to emphasise that the obtained results are similar to the previous work of Rada et al. [25, 23] overcoming the previous work of Gout et al. [12] and [3]. For briefness, we do not show the results obtained by the previous work of Rada et al. [25, 23, 24] but we note that both models give the same satisfactory results as shown in Fig. 1. For more details reader can refer to the results shown in [25, 23, 24] papers. Based on the same papers [25, 23], the results shown in Fig. 1 have the same results by Nguyen et al. [21] model given a proper initialization. In the following, we show test results where the proposed model performs better than Nguyen et al. [21] model. Comparison to Rada et al. [25, 23] work for such images is not shown as the obtained results are the same for such cases. Fig. 2 shows the comparison results between Rada et al. [25], Nguyen et al. model [21] and the proposed model for a Christmas tree in a pot and cell image in the first and the second row, respectively. We can easily notice successful results by Rada et al. [25] and the new model for a real-life image of a Christmas tree in a pot where the nearby pixels have different intensities in an oscillatory structure. The Nguyen et al. model [21] can sufficiently good capture the tree but fails to capture the whole pot due to semi-transparent boundaries. Nguyen et al. model [21] fails also to segment the nearby cell images, as shown in the second row due to the fact that the cells are of the same intensity and separated with one pixel between them. Fig. 2 show that Nguyen et al. [21] method cannot handle transparent or semi-transparent boundaries and noise. ,s figure we can clearly see that our method and Rada et al. [25] properly segment such cases.

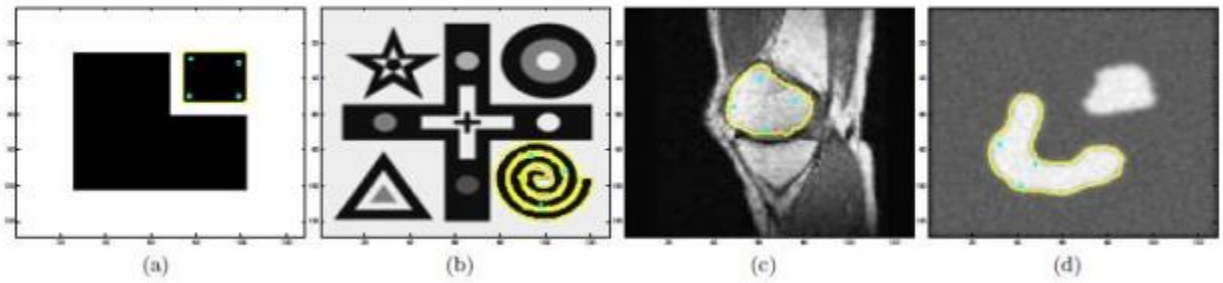

Figure 1. Test Set 1 – Successful segmentation of different images with the proposed method with given markers in blue color.

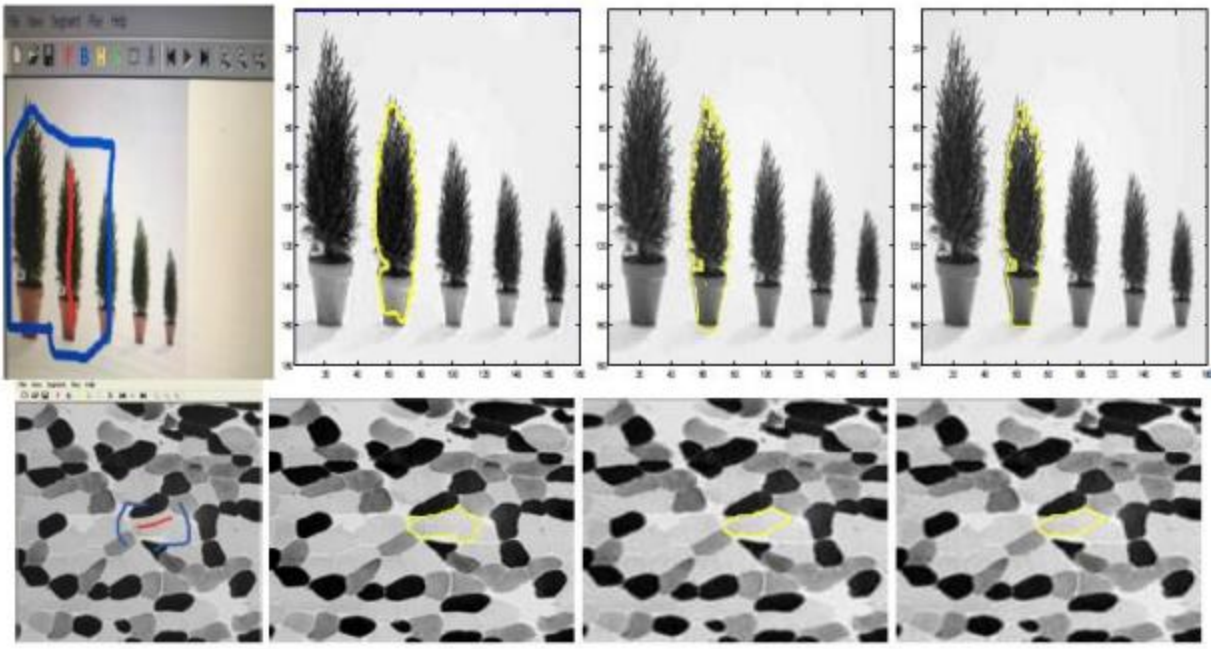

Figure 2. Test Set 1 – Comparison with Rada et al. [25] and Nguyen et al. model [21] for a Christmas tree in a pot and cell images in the first and the second row respectively.

Test Set 2 — Comparison with The Rada Et Al. [24] Model

The second set of experiments compares the proposed model with the infinite perimeter dual level set selective (IPDLSS) method [24] and show similar results for oscillatory boundaries by gaining a better performance speed. We demonstrate the ability of the new model to recognize specific objects with oscillatory boundaries while the proposed method has priority in terms of CPU time. In particular, we consider trees segmentation since the cornering effect of the model can be observed and the characteristic of these images is oscillatory boundaries.

Figs. 3, 4, and 5 show the compared results of the new model with the previous work of Rada et al. [23, 24]. Fig. 3 show the comparison of the model with Rada et al. [23]. Both models have the same speed of convergence and similar results. The speed of convergence is similar as both models run over one level set. In comparison with Rada et al. [24] model, we can notice that the proposed model performs accurate results for low-quality oscillatory data, similar to the previous work of Rada et al. [24] model and outperforms the Rada et al. [23] model as shown in Fig. 4. Looking into the segmentation results of those images, we can notice that the previous Rada et al. [23] model will lose some details between the tree's branches, see Fig. 5, taken from Fig. 4 left corner crop. We acknowledge that the parameter used for all the experiments are fixed as given at the beginning of this section. For better performance of the proposed method, the tuning of the parameters is required, such as the increase of the parameter k for better details in case of oscillatory boundary. In the following, we show the priority of the proposed method compared to the IPDLSS model [24] in terms of the speed of the convergence. IPDLSS model suffer from a slow convergence due to the fact that successively must update the global and local level sets. Table 1 shows clearly this fact. In this table, we compare the CPU time of new model with the old IPDLSS model [24] and find out that the new model is at least two times faster. In this table we show the results of 6 images but we acknowledge that similar results to Table 1 were obtained in all performed experiments without exceptions.

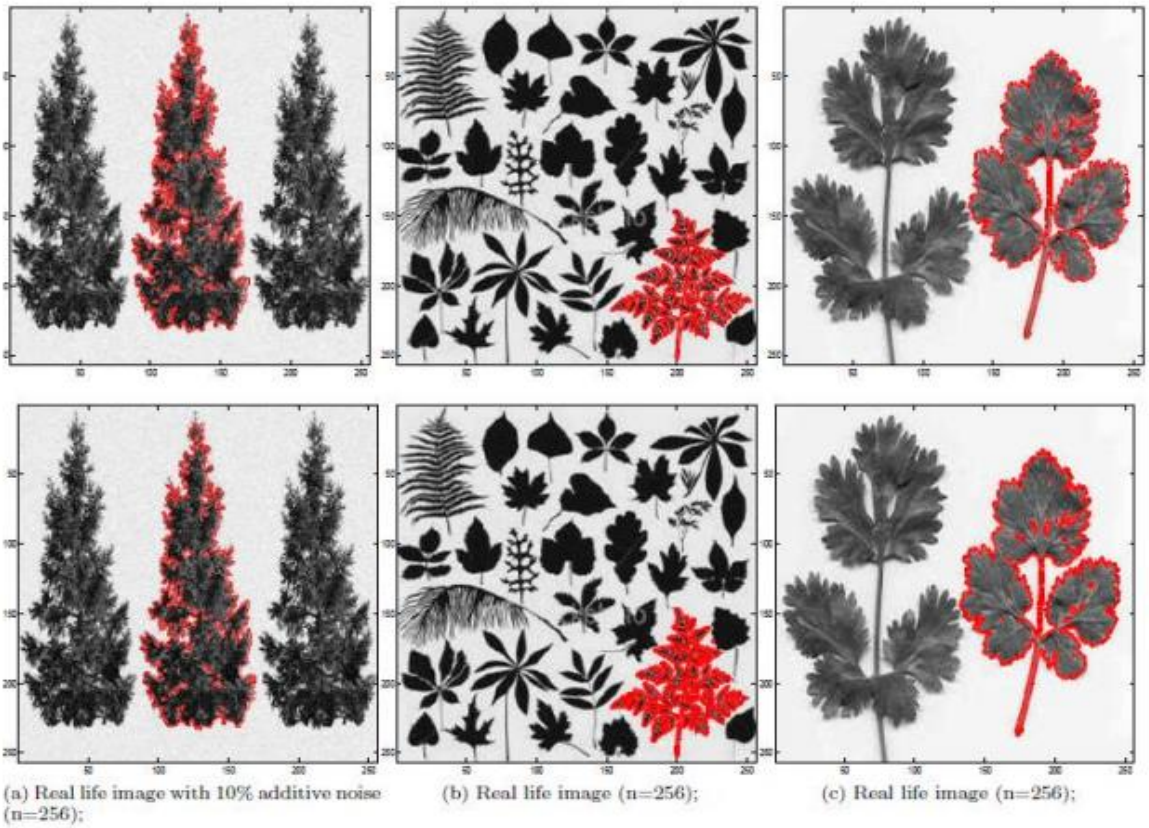

Figure 3. Segmentation results for Rada et al. [23, 24] models and the proposed selective segmentation model. The first column show the results obtained from Rada et al. [23] model, the second column the results obtained from Rada et al. [24] and the last column the obtained results with the new model.

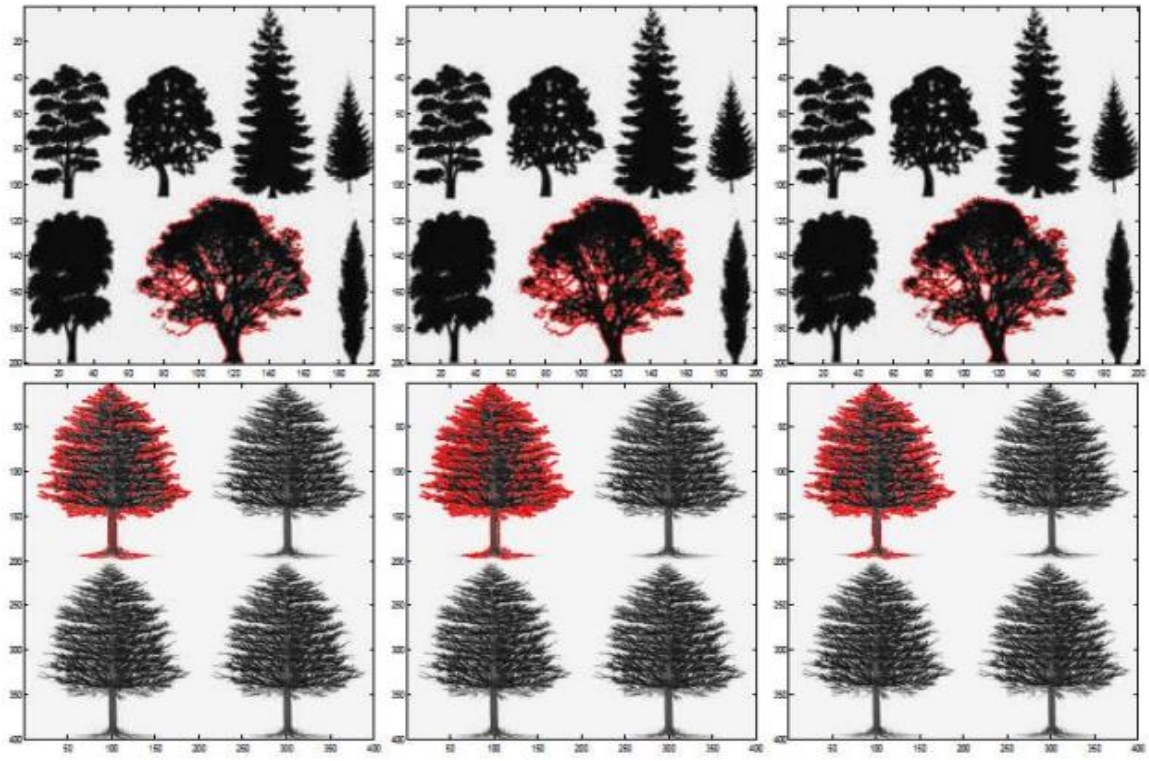

Figure 4. Segmentation results for Rada et al. [23, 24] models and the proposed selective segmentation model. The first column show the results obtained from Rada et al. [23] model, the second column the results obtained from Rada et al. [24] and the last column the obtained results with the new model.

Figure 5. Segmentation results for Rada et al. [23, 24] models and the proposed selective segmentation model. The first column show the results obtained from Rada et al. [23] model, the second column the results obtained from Rada et al. [24] and the last column the obtained results with the new model.

Table 1. Required CPU time for the proposed method and ist comparison to IPDLSS.

Figure	IPDLSS method CPU time	New method CPU time
Img. 1(256 × 256)	58.7938	16.3198
Img. 2(256 × 256)	49.5213	17.1265
Img. 3(256 × 256)	46.1250	17.7688
Img. 4(256 × 256)	35.4201	16.2090
Img. 5(256 × 256)	49.120	18.8890
Img. 6(256 × 256)	31.7601	17.8190

Test Set 3 — Useful Applications for Data Boundary Refinement

In this experiment, we show some useful applications where clearly the proposed model qualitatively refines the aimed boundaries. In this experiment, we use a public accessible PH2 dataset [31] consisting of 200 skin cancer images. The database collection was a collaboration between the Dermatology Service of Hospital Pedro Hispano in Matosinhos, Portugal, and The Universidade do Porto in Ecnico Lisboa. The database has two files: one of the files with the original image and another one consisting of lesion boundaries drown by the specialist of the field in a mechanical time-consuming process. We used this dataset to show that we can help the specialist correctly capturing and refining the lesion boundaries. Figs. 6 and 7 show the segmentation results of the proposed method compared with boundaries drawn by the specialist. In Fig. 6, we notice that there is a similar output of the drawn boundaries between the specialist, in the first row, and the proposed method, in the second row, whereas Fig. 7 show results where the proposed method can better distingue between healthy and non-healthy regions of the lesion. Such a result would be of help especially if laser-like techniques are used to burn the non-healthy cells.

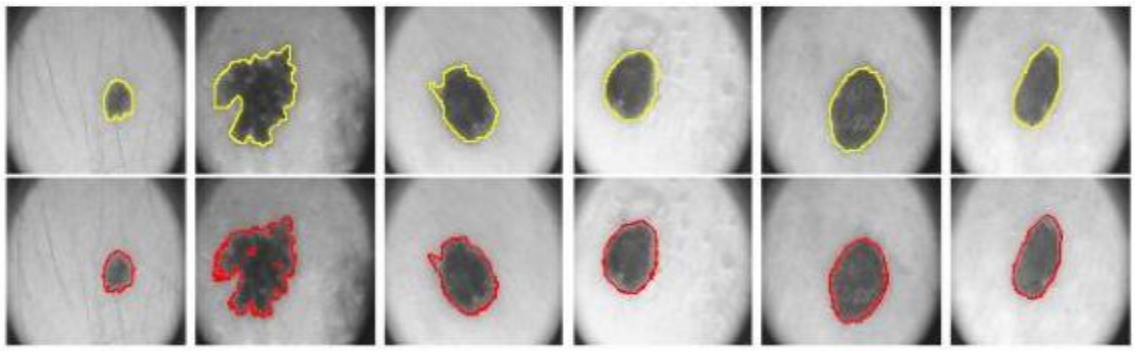

Figure 6. Segmentation results comparison for the original segmented lesion boundaries (made by a specialist) in the first row and the proposed method in the second row.

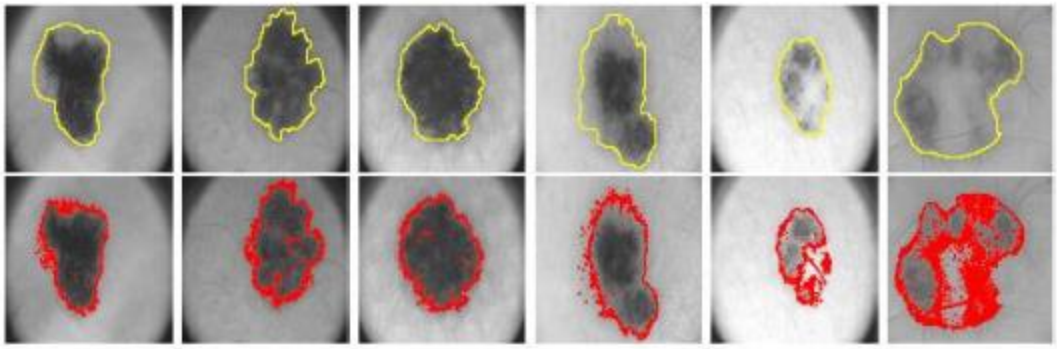

Figure 7. Segmentation results comparison for the original segmented lesion boundaries (made by a specialist) in the first row and the proposed method in the second row.

6. CONCLUSIONS

The presented variational selective segmentation model show reliable segmentation for the aimed object of interest with oscillatory boundaries. This model delivers similar results to old models, such as the Rada et al. model [24, 23] or better results for oscillatory boundaries compared to [25] and Nguyen et al. [21] model. The model improves the convergence speed of the Rada et al. [24] model by having the same accuracy for oscillatory boundaries objects. To indicate the significant contribution of this study we show some real-life applications using PH2 open-source dataset [31] with medical images where cancer segmentation is required. We can easily see through experiments that the proposed method has a really good quantitative segmentation.

7. REFERENCES

1. G. Aubert and P. Kornprobst. "Mathematical problems in image processing: Partial Differential Equations and the Calculus of Variations," Springer, 2001. ""

2. V. Badrinarayanan, A.Kendall, and R. Cipolla. "Segnet: A deep convolutional encoder-decoder architecture for image segmentation," CoRR., 2015.

3. N. Badshah and K. Chen. "Image selective segmentation under geometrical constraints using an active contour approach," Commun. Comput. Phys., 7(4):759–778, 2009.

4. M. Barchiesi, S. H. Kang, T. M. Le, M. Morini, and M. Ponsiglione. "A variational model for infinite perimeter segmentations based on lipschitz level set functions: Denoising while keeping finely oscillatory boundaries," Multiscale Modeling & Simulation, 8(5):1715–1741, 2010.

5. G. J. Brostow, J. Fauqueur, and R. Cipolla. "Semantic object classes in video: A high-definition ground truth database," Pattern Recogn. Lett., 2:88–97, 2009.

6. V. Caselles, R. Kimmel, and G. Sapiro. "Geodesic active contours. International Journal of Computer Vision," 22(1):61–79, 1997.

7. T. F. Chan and L. A. Vese. "Active contours without edges," 1998.

8. L. C. Chen, G. Papandreou, I. Kokkinos, K. Murphy, and A. L. Yuille. Deeplab: "Semantic image segmentation with deep convolutional nets, atrous convolution, and fully connected crfs, " IEEE Transactions on Pattern Analysis and Machine Intelligence, 40(4):834–848, 2018.

9. D. Comaniciu, P. Meer, and S. Member. "Mean shift: A robust approach toward feature space analysis" IEEE Transactions on Pattern Analysis and Machine Intelligence, 24:603–619, 2002.

10. S. Geman and D. Geman. "Stochastic relaxation, gibbs distributions and the bayesian restoration of images," IEEE Transactions on Pattern Analysis and Machine Intelligence, (6):721–741, November.

11. C. Gout, C. Le Guyader, and L. A. Vese, "Segmentation under geometrical consitions with geodesic active contour and interpolation using level set methods," Numerical Algorithms, 39:155–173, 2005.

12. C. Gout. "Viscosity solutions for geodesic active contour under geometrical conditions," International Journal of Computer Mathematics, 85(9):1375–1395, 2008.

13. C. Le Guyader and C. Gout. "Geodesic active contour under geometrical conditions theory and 3d applications," Numerical Algorithms, 48:105–133, 2008.

14. Steve Hanov. "Wavelets and edge detection," April 2006.

15. T. Lu, P. Neittaanmaki, and X. C. Tai. "A parallel splitting-up method for partial differential equations and its application to navier-stokes equations," RAIRO Mathematical Modelling and Numerical Analysis, 26(6):673–708, 1992.

16. J. Malik, Th. Leung, and J. Shi. "Contour and texture analysis for image segmentation," International Journal of Computer Vision, 43:7–27, 2001.

17. S. Mallat. "A wavelet tour of signal processing, "Academic Press, USA, 1998.

18. P. Morrow, S. McClean, and K. Saetzle. "Contour detection of labeled cellular structures from serial ultrathin electron microscopy sections using gac and prior analysis," IEEE Proceedings of IPTA, pages 1–7, 2008.

19. D. Mumford and J. Shah. "Optimal approximation by piecewise smooth functions and associated variational problems," Communications on Pure Applied Mathematics, 42:577–685, 1989.

20. D. Mumford and J. Shah. "Boundary detection by minimizing functionals," In IEEE Conference on Computer Vision and Pattern Recognition.

21. T. Nguyen, J. Cai, J. Zhang, and J. Zheng. "Robust interactive image segmentation using convex active contours," IEEE Transactions on Image Processing, 21:3734–3743, 2012.

22. S. Osher and J. A. Sethian. "Fronts propagating with curvature dependent speed: Algorithms based on hamilton-jacobi formulations," Journal of Computational Physics, 79(1):12–49, 1988.

23. Lavdie Rada and Ke Chen. "Improved selective segmentation model using one level-set," Journal of Algorithms & Computational Technology, 7(4):509–540, 2013.

24. Lavdie Rada and K. Chen. "On a variational model for selective image segmentation of features with infinite perimeter," volume 33, pages 253–272, 2013.

25. L. Rada and K. Chen. "A new variational model with dual level set functions for selective segmentation," CiCP, 12(1):261–283, 2012.

26. D. Sen and S. K. Pal. "Histogram thresholding using fuzzy and rough measures of association error," Image Processing, IEEE Transactions on, 18(4):879–888, 2009.

27. N. Valliammal and S. N. Geethalakshmi. "Performance analysis of various leaf boundary edge detection algorithms," In Proceedings of the 1st Amrita ACM-W Celebration on Women in Computing in India, A2CWiC '10, pages 34:1–34:6, 2010.

28. J. Weickert and G. Kühne. "Fast methods for implicit active contour," In N. Paragios S. Osher, editor, Geometric Level Set Methods in Imaging, Vision, and Graphics, pages 43–57. Springer New York, 1995.

29. J. Weickert, B.M. Romeny, and M.A. Viergever. "Efficient and reliable schemes for

nonlinear diffusion filtering," IEEE Transactions on Image Processing, 7(3):398–410, 1998.

30. Xiangrong Zhang, Feng Dong, G. Clapworthy, Youbing Zhao, and Licheng Jiao. "Semi-supervised tissue segmentation of 3d brain mr images," In Information Visualisation (IV), 2010 14th International Conference, pages 623 –628, 2010.

31. T. Mendonça, P. M. Ferreira, J. S. Marques, A. R. S. Marcal and J. Rozeira, "PH2 - A dermoscopic image database for research and benchmarking," 2013 35th Annual International Conference of the IEEE Engineering in Medicine and Biology Society (EMBC), 2013, pp. 5437-5440.